UCID-21179

Thermal Damage Study of Beryllium Windows Used as Vacuum Barriers in Synchrotron Radiation Beamlines

F. R. Holdener, G. L. Johnson,
V. P. Karpenko, and P. K. Wiggins

Lawrence Livermore National Laboratory

J. A. Cerino, M. T. Dormiani, and B. P. Youngman

Stanford Synchrotron Radiation Laboratory

E. W. Hoyt

Stanford Linear Accelerator Center

September 17, 1987

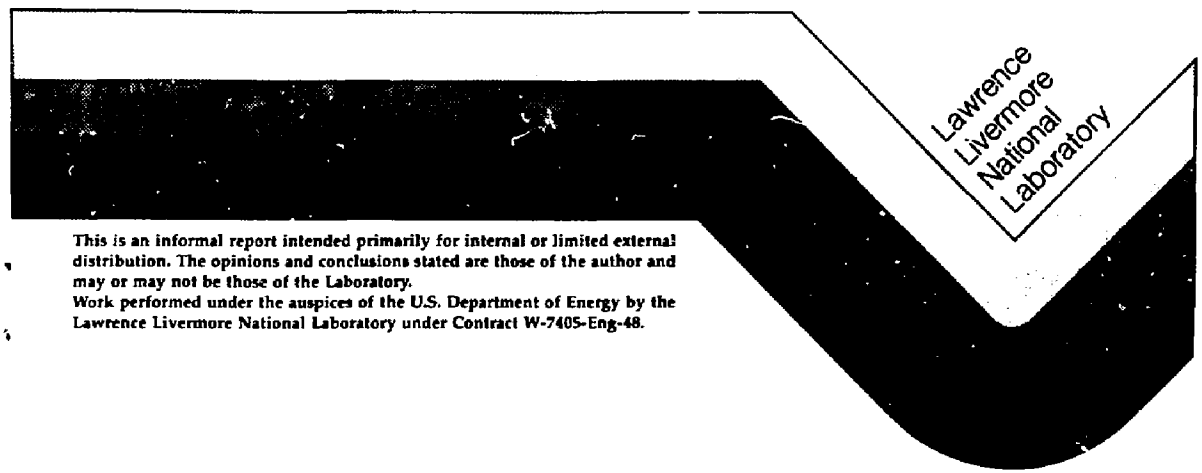

UCID--21179

DE88 002655

CONTENTS

THERMAL DAMAGE STUDY OF BERYLLIUM WINDOWS USED AS VACUUM BARRIERS IN SYNCHROTRON RADIATION BEAMLINES

ABSTRACT

An experimental study to investigate thermal-induced damage to SSRL-designed beryllium foil windows was performed at LLNL's Laser Welding Research Facility. The primary goal of this study was to determine the threshold at which thermal-stress-induced damage occurs in these commonly used vacuum barriers. An Nd:Yag pulsed laser with cylindrical optics and a carefully designed test cell provided a test environment that closely resembles the actual beamline conditions at SSRL. Tests performed on two beryllium window geometries, with different vertical aperture dimensions but equal foil thicknesses of 0.254 mm, resulted in two focused total-power thresholds at which incipient damage was determined. For a beam spot size similar to that of the Beamline-X Wiggler Line, onset of surface damage for a 5-mm by 25-mm aperture window was observed at 170 W after 174,000 laser pulses (1.2-ms pulse at 100 pps). A second window with double the vertical aperture dimension (10 mm by 25 mm) was observed to have surface cracking after 180,000 laser pulses with 85 W impinging its front surface. It failed after approximately 1,000,000 pulses. Another window of the same type (10 mm by 25 mm) received 2,160,000 laser pulses at 74.4 W, and subsequent metallographic sectioning revealed no signs of through-thickness damage. Comparison of windows with equal foil thicknesses and aperture dimensions has effectively identified the heat flux limit for incipient failure. The data show that halving the aperture's vertical dimension allows doubling the total incident power for equivalent onsets of thermal-induced damage.

INTRODUCTION

Beryllium windows are a key component of beamlines used for synchrotron radiation research. At the present, all but one of the double-crystal monochromators at Stanford Synchrotron Radiation Laboratory (SSRL) work in an environment of one atmosphere of helium (He). This necessitates a beryllium (Be) window upstream from the monochromator to isolate the monochromator

chamber from the electron storage ring which is at 10^{-9} Torr. These Be windows limit the photon flux of the wiggler beamlines in the Stanford Positron Electron Accelerator Ring (SPEAR).

Due to concerns of possible Be window failure if the existing calculated 3.75 W/mm line-load thermal flux (equivalent to 3.75 W/mm^2 for a 1-mm beam spot width) window limit is exceeded, there are two 0.254-mm (0.010-in.) thick windows upstream from the monochromator with the interspace filled with argon at 0.5 atm. This interspace is continuously monitored to detect a possible leak from either window. To protect the windows from overheating, graphite filters are installed upstream from the windows.

At a stored electron energy of 3 GeV, the critical energy of the wiggler is approximately 7.8 keV. This means that half the power emitted from the electrons is at energies less than 7.8 keV. The absorption of even 0.025 mm (0.001 in.) of beryllium or carbon is nearly 100% at energies less than 1 keV. Thus, absorbing soft x ray and vacuum ultraviolet (VUV) light with carbon filters protects the Be windows while transmitting the harder portion of the synchrotron spectrum. Nonetheless, there would be up to 50% more flux available for researchers at 7.8 keV if one could remove both the beryllium and carbon from the beamline. It is desirable to reduce the thickness of existing window designs in order to obtain greater flux throughput. The effort to understand potential causes of Be failure could lead to thinner window designs with the possibility of eliminating one of the two windows in the redundant double-window design.

BEAM CHARACTERISTICS

Beamline-X, a wiggler/undulator x-ray source presently nearing construction completion at SSRL, has Be window requirements typical of other beamlines at SSRL, e.g., Beamline-VI. The basic Beamline-X optical configuration is shown schematically in Fig. 1, with system parameters listed in Table 1. For a 15-period wiggler at 1.3 tesla with a 128.7-mm period length and an electron energy of 3 GeV and a critical energy of 7.78 keV, the cross section of the source beam is essentially an elongated ellipse with 2-σ (standard deviation of an ideal Gaussian distribution) dimensions of 0.4 mm by 5 mm. The resulting beam shape at the Be window is a typical "smile" (see Fig. 1). The smile's basic 2-σ dimensions are 1.3 mm by 15.8 mm.

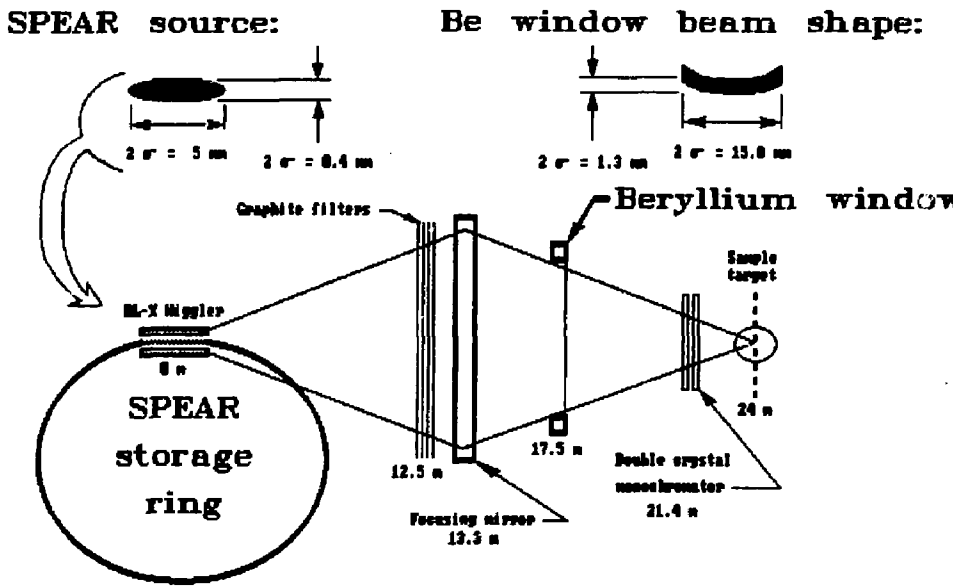

Figure 1. Beamline-X optics configuration with the beam shape at the Be window for wiggler beamline parameters listed in Table 1.

Table 1. System parameters for Beamline-X analysis.

Wiggler
Peak field: 1.3 Tesla
Number of periods: 15
Period length: 128.7 mm
Length: 2.1 m
SPEAR ring
Beam current: 100 mA
Electron energy: 3.0 GeV
Horizontal source size: 5.0 mm FWHM
Vertical size: 0.4 mm FWHM
Beamline
Graphite filter: location 12.5 m[a]
Thickness 0.254 mm (10 mils)
Focusing mirror: location 13.3 m
Grazing angle 0.2 deg (3.5 mrad)
Length 700 mm
Short radius 41.4 mm
Long radius 3400 m
Focal spot location 24 m
Be window: location 17.5 m
Thickness 0.406 mm (16 mils)
First crystal: location 21.4 m

[a]Component location is relative to the wiggler center.

GOALS OF THE EXPERIMENT

The experimental goals of this study are to:

1. Simulate beamline conditions in a laser thermal cycling test setup for Be windows.

2. Quantify the number of laser pulses and the beam power level (i.e., beam energy density per unit time) for the onset of window damage. Onset of window damage is defined as a visually detectable change in surface characteristics.

3. Identify the beam power level and number of pulses where window failure occurs. Failure is defined as perforation of the window, allowing gas exchange or loss of forward chamber vacuum.

4. Ascertain the mode of window failure and understand what metallurgical or structural flaws account for failure.

DESCRIPTION OF EXPERIMENTAL APPARATUS

SSRL provided the beryllium windows for the thermal damage study performed at LLNL's Laser Welding Facility. The windows were fabricated by Electrofusion (Fremont, California) per SSRL specifications. The two window types tested, both 0.254-mm thick, have apertures of 5 mm by 25 mm and 10 mm by 25 mm, respectively. The window aperture is oriented in this test the same way as in Beamline-X, i.e., with the long dimension of the window on the horizontal and the Be foil normal to the incident beam axis. The beryllium foil is vacuum brazed into a copper heat sink (see Fig. 2). The heat sink has a 5-mm stainless steel tube soldered into a groove on its perimeter for water cooling. The Be window is mounted at the beam exit side of the copper aperture. The high-purity beryllium (grade IF-1 consisting of 99.8% Be) is produced by extruding and hot rolling beryllium ingots cast from vacuum-melted, electrolytically refined beryllium flakes.

The Be window assembly is mounted into a special test cell shown schematically in Figs. 3 and 4. The Be foil separates the test cell into two chambers, each of which may be independently pressurized or evacuated. The forward chamber provides space between the Be window and the sapphire window laser beam inlet port. The rear chamber extends from the Be window to the rear sapphire window at the observation port. Each chamber is sealed to the Be window assembly by O-ring seals and fitted with a line to which a vacuum pump and a gas pressure source (argon or helium) are connected. Both chambers are monitored with a vacuum transducer and a pressure gage.

The laser beam source is a Raytheon Model SS-501-A7 Precision Welder/Driller. Specific parameters of this unit are given in Table 2. The workpiece table moves in the x-y or horizontal plane. The laser beam exit aperture moves in the z or vertical axis. The workpiece table and the laser beam head movement are accurately positioned by computer numerical control (CNC) with accuracy of $< \pm 0.003$ in. The test cell, calorimeter, infrared camera, and vacuum/pressure valves and vacuum gages are mounted on the x-y table (see Figs. 5 through 7). Each piece of equipment is assigned an x-y-z set position with the CNC system for easy realignment.

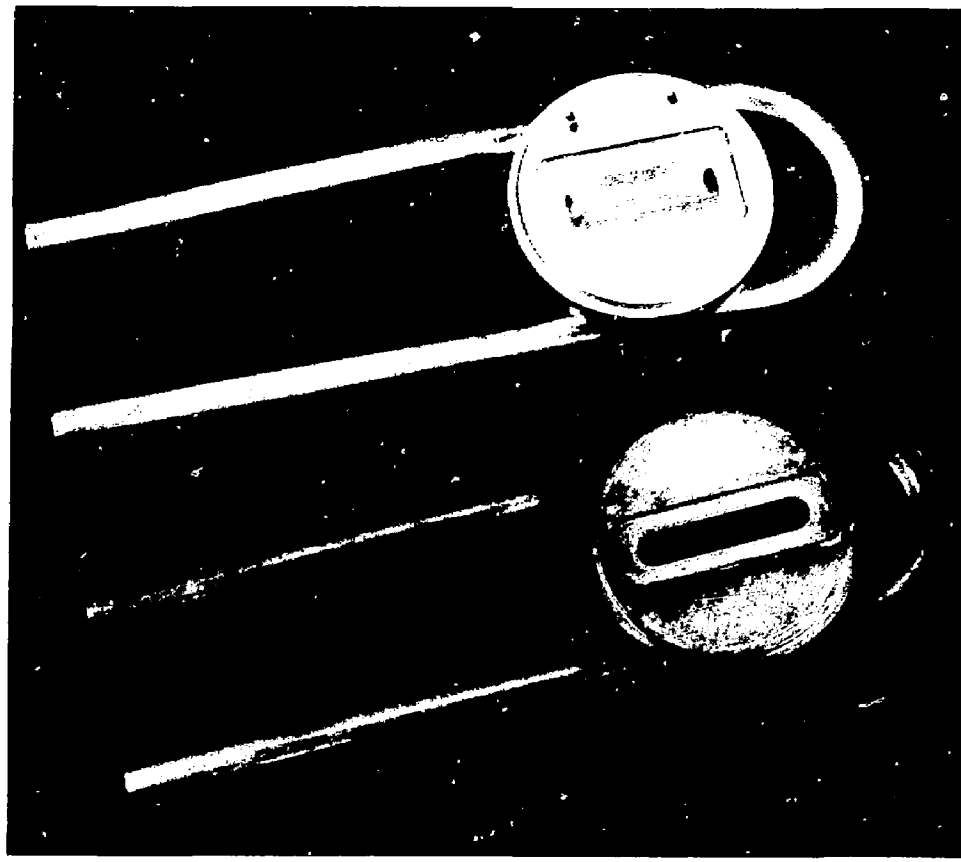

Figure 2. Beryllium window assemblies consisting of 0.254-mm beryllium foil vacuum brazed into a copper heat sink that has a 5-mm stainless steel tube soldered into its perimeter groove: (a) 10-mm by 25-mm aperture shown with Be foil mounted, (b) 5-mm by 25-mm aperture with Be foil removed.

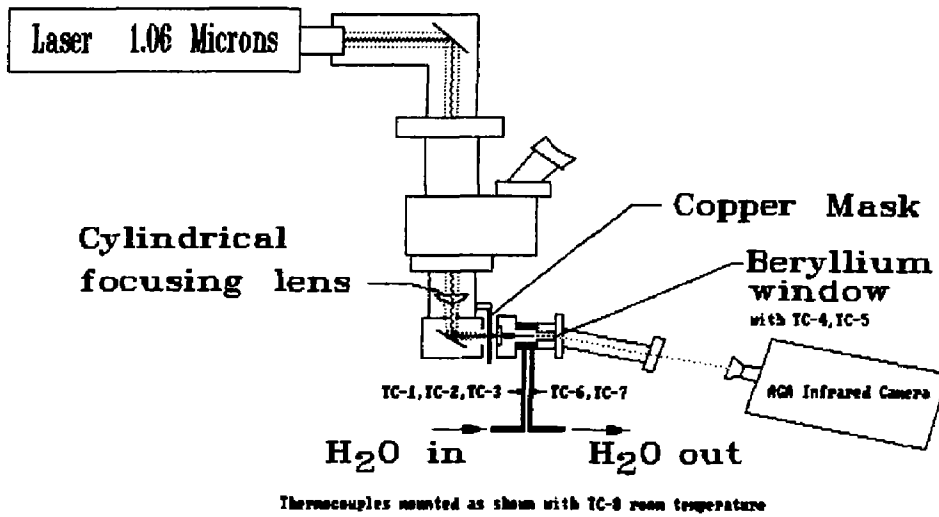

Figure 3. Laser-impinged beryllium window thermal test schematic showing key components: AGA infrared camera, spectral range of 3 to 6 μm; thermocouples; cylindrical focusing lens, uncoated fused silica, 150-mm focal length; laser parameters are listed in Table 2.

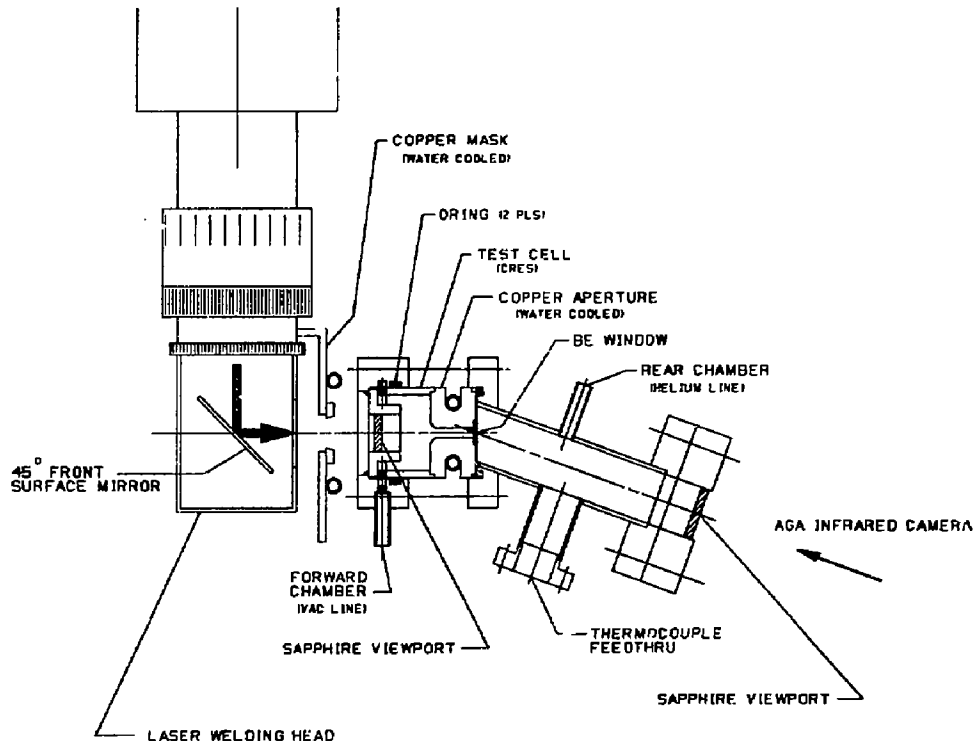

Figure 4. Beryllium window test cell schematic showing detailed cross section.

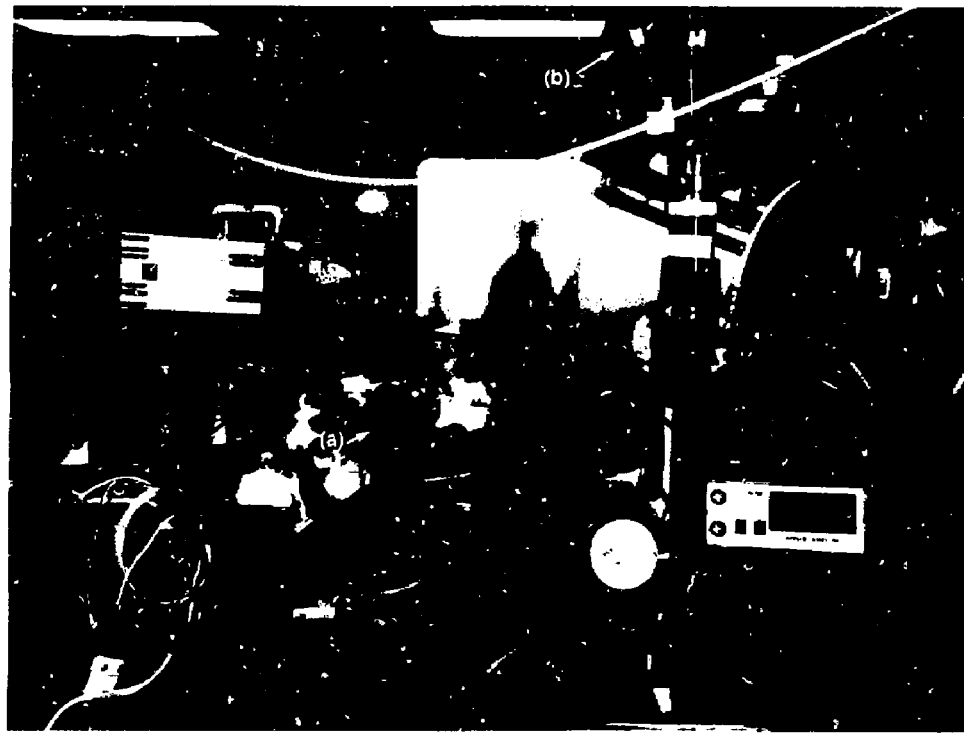

Figure 5. Photograph of actual Be window test setup showing: (a) front view of test cell, (b) Nd:Yag laser source and associated diagnostics.

Figure 6. Photograph of Be window test setup showing vacuum pump, water flow system and associated controls.

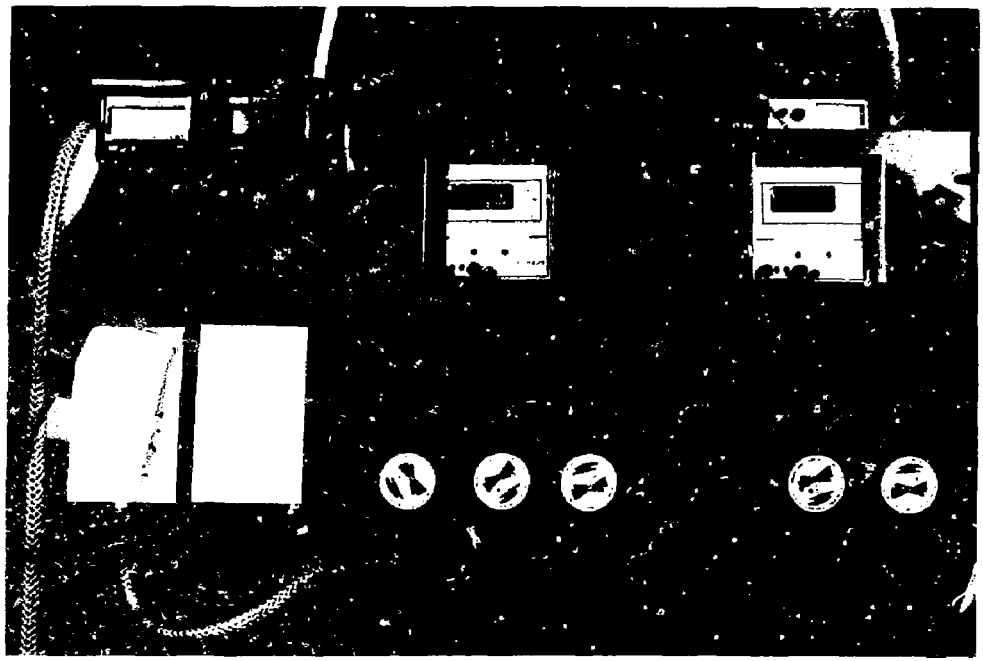

Figure 7. Photograph of Be window test control panel with vacuum-to-pressure controls and associated readouts.

Table 2. Parameters of Raytheon Model SS-501B-A7 precision welder/driller.

Rated average power	400 W
Rated maximum pulse energy	50 J
Pulse rate, continuously variable	1-200 pulses/s
Beam spot diameter	0.2 - 2.0 mm
Wavelength	1.06 μm
Output power regulation	± 5%
Pulse width, incrementally variable	7 ms

For all tests the pulse width was set at 1.2 ms and the pulse rate was set at 100 pulses/s. A pulse-forming network adjusts the total energy stored per pulse and thus the laser power output. The spherical focusing lens normally used for welding/drilling operations was replaced with an uncoated 150-mm cylindrical fused silica lens. The lens focuses the laser beam in the vertical direction, closely approximating the actual synchrotron wiggler beam spot size but without the characteristic smile resulting from the actual beamline cylindrical mirror. The beam is reflected horizontally with a 45-degree front surface mirror and then passes through a water-cooled copper mask that removes the outer beam edges producing the desired beam dimensions. The laser beam then passes through the test chamber's front sapphire window and onto the Be window surface.

A target block is mounted to the side of and in the same plane as the Be window in order to check the beam spot size attained. Exposed photographic paper mounted to the target block was burned with the laser beam to document the actual spot size and shape on the Be foil (see Fig. 8 for examples of beam burns).

An AGA Thermovision 780 infrared camera system monitored the relative temperature gradients and heat flow patterns on the back of the Be through the observation port. The camera uses a shortwave scanner sensitive to the 3.0-to-5.6 μm spectral band. Figure 9 shows typical outputs in color-band gradients of windows 2A and 2B. Besides verifying laser beam centering, the AGA camera also gives a rough definition of the temperature gradients on the window. To interpret the camera output of Fig. 9b according to the AGA camera operations manual, one adds the thermal level setting (in this case 40 isothermal units) to the color band reading (e.g., white marker at 0.10) times the thermal range (set in this case at 500). The result, 40 + (0.1*500) = 90 isotherm units, yields a temperature of 145°C from the calibrated curve in Fig. 10. In this manner temperatures can be obtained at any location on the window.

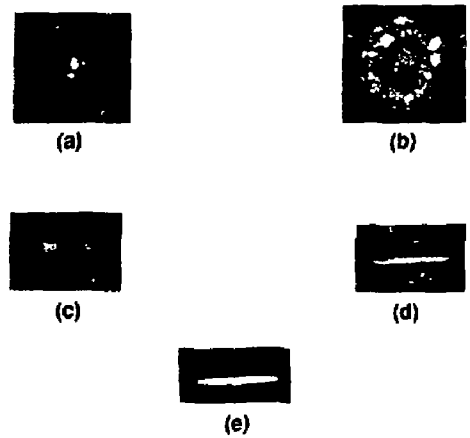

Figure 8. Actual beam burns of exposed photographic paper with 10 laser pulses for 0.1-s shutter duration: (a) unfocused beam at 100 W, (b) unfocused beam at 200 W, (c) semi-focused beam at 100 W, (d) focused beam at 100 W, (e) focused beam at 200 W.

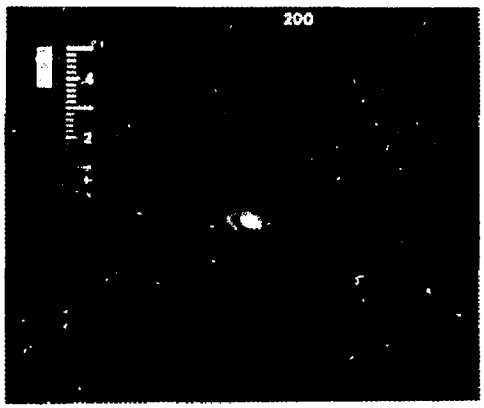

(a)

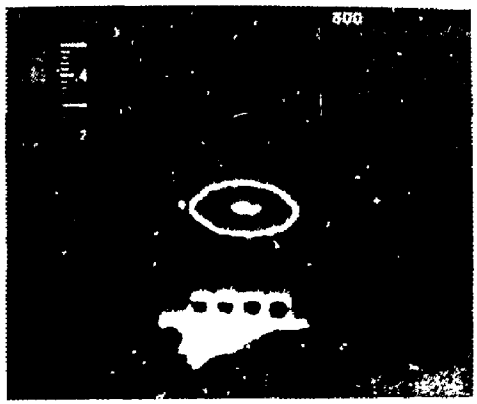

(b)

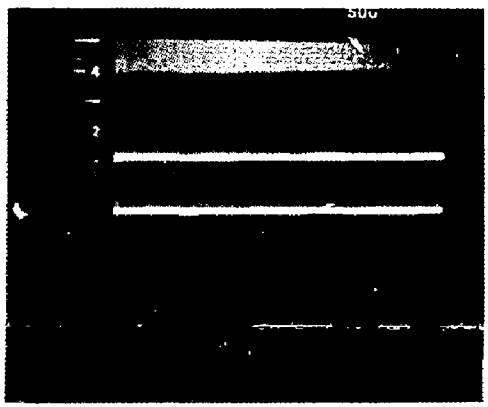

(c)

Figure 9. Samples of AGA infrared photographic data for 10-mm by 25-mm apertures at two different power levels: (a) 74 W impinging window 2B with white isotherms shut off, (b) 85 W impinging window 2A with isotherms turned on, (c) color bars corresponding to temperatures of (b).

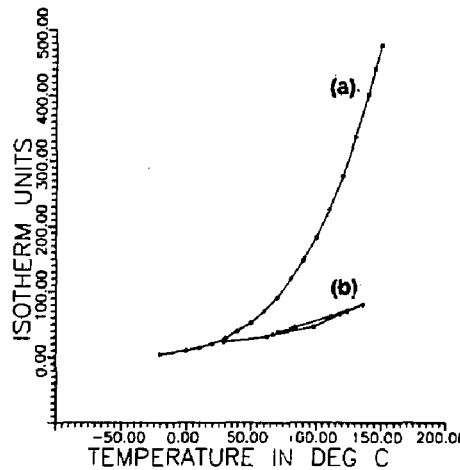

Figure 10. Calibration curves for the AGA infrared camera: (a) top curve was obtained from operations manual for ideal blackbody, (b) bottom curve was measured with actual test cell wrapped with heater tape and well insulated. Average temperatures from thermocouples TC-4 and TC-5 were recorded and plotted against AGA camera readings observed on the Be surface between the two thermocouples.

Calibration curves shown in Fig. 10 were obtained from two sources. The AGA Camera manufacturer provided the top (blackbody) curve in its operations manual. The bottom curve was obtained by wrapping the test cell with heater tape, insulating it, and reading the thermocouple temperatures on the Be along with the thermal isothermal units from the AGA Camera. The emissivity of the Be as measured in the AGA shortwave scanner's 3-to-6 μm spectral range is a function of temperature. The ratios for real to blackbody values (i.e., measured emissivities) are 0.55, 0.30, and 0.20 for temperatures of 50°C, 100°C, and 150°C, respectively. These emissivity values seem reasonable, but need further study if used to do any extensive analysis.

System temperatures were monitored by thermocouples as schematically shown in Fig. 3. The back surface temperature of the Be foil was measured by two 0.03-mm (1-mil) thermocouples spot welded to the back surface. Thermocouple four (TC-4) was mounted 6.5 mm horizontally off-center. TC-5 was mounted on the geometric center of the Be window. TC-5 reads the hot spot back surface temperature of the centered laser beam as it impinges on the front of the Be window. TC-1, TC-2, and TC-3 read the temperature of the water entering the test cell, while TC-6 and TC-7 read the exit water temperature. TC-8 reads room temperature. A Hanzon 4000 Series Digital Readout Data Logger with a Hewlett Packard Thinkjet Printer recorded thermocouple time-temperature data. Figure 11A shows a photo of the instrumentation and Fig. 11B a sample printer output of the peak temperature data taken for windows 1, 2A, and 2B.

Energy of the laser was measured directly by dumping the beam into a calorimeter (Apollo Lasers Inc., Model ALC and associated readout, Model ACM-101). Laser pulse rate in pulses per second (pps) was determined with an oscilloscope connected to a detector directly on the laser rod.

Argon gas is supplied from a regulated building central supply system. The helium gas source is from a helium bottle with a standard regulator. Both gas sources are regulated a second time with precision low-pressure regulators. These regulators are set at 15.1 psia (0.4 psig) pressure.

System gas valves were Nupro bellows valves qualified to 1×10^{-6} std cm^3 He/min leak rate. The vacuum system consisted of a Welch rotary-vane vacuum pump with a liquid nitrogen foreline trap. This vacuum system normally provided a millitorr level vacuum. Two Granville-Philips Series 275 Digital Readout Convectron Vacuum Gages read in the vacuum-to-pressure range on each side of the test cell.

Figure 11A. Photograph of Be window test instrumentation showing: (a) AGA camera console, (b) Hanzon 4000 series digital temperature readout/data logger, (c) HP Thinkjet printer connected to Hanzon, (d) color monitor for AGA camera, (e) large console in center is X-Y-Z CNC control console, (f) large console to the right is the controller for the Raytheon laser with system parameters listed in Table 2.

```
27 Mar 87   09:54:48
CH001=+064.0 Deg F      HI
CH002=+064.5 Deg F      OK
CH003=+064.8 Deg F      OK
CH004=+307.7 Deg F      OK
CH005=+666.1 Deg F      HI
CH006=+127.3 Deg F      OK
CH007=+130.1 Deg F      OK
CH008=+067.1 Deg F      OK
```

(a) Window Number 1 Data

```
09 Apr 87   14:45:01
CH001=+064.0 Deg F      HI
CH002=+064.5 Deg F      OK
CH003=+065.1 Deg F      OK
CH004=+343.1 Deg F      OK
CH005=+717.8 Deg F      HI
CH006=+389.2 Deg F      OK
CH007=+089.7 Deg F      OK
CH008=+065.9 Deg F      OK
```

(b) Window Number 2A Data

```
22 Apr 87   12:53:08
CH001=+064.0 Deg F      HI
CH002=+064.0 Deg F      OK
CH003=+064.0 Deg F      OK
CH004=+276.3 Deg F      OK
CH005=+445.5 Deg F      OK
CH006=+084.6 Deg F      OK
CH007=+078.3 Deg F      OK
CH008=+062.4 Deg F      OK
```

(c) Window Number 2B Data

Figure 11B. Samples of data from Hanzon-4000/HP-Thinkjet for peak temperatures on windows 1, 2A, and 2B. Thermocouples TC-1, TC-2, and TC-3 read water temperature entering the test cell; TC-4 reads the back surface temperature of Be window at 6.5-mm horizontally off-center; TC-5 reads the back surface temperature of the center "hot spot" of the Be window; TC-6 and TC-7 read water temperature exiting the test cell; TC-8 reads room temperature. (Channel numbers correspond to the thermocouples.)

A Masterflex variable speed pump (97 ml/min maximum flow rate) from Cole Parmer controlled the flow rate of cooling water to the test cell. Most tests were run with 10°C to 20°C temperature rise between supply and return of the Be window cooling water.

A Nikon long-focal-length microscope, typically known as a "surgeons microscope," was used to look at the Be window within the test cell. With this unit, the slightest change of surface characteristics was readily observed.

DESCRIPTION OF THE EXPERIMENT

The experimental parameters are: beam size and shape, beam power, laser pulse shape and rate, coolant flow rate to the test cell, test cell chamber pressures, and window illumination time intervals. Beam shape is rectangular, measuring approximately 2-mm wide by 14-mm long in size. It is oriented on the window with its long axis corresponding to the horizontal axis of the window aperture. Laser pulse shape and rate are set close to maximum laser power conditions and as close to steady-state as is reasonably possible. The laser runs well for long periods at 100 pps, but is much less stable at the higher pulse rates. Therefore the 100 pps rate became the standard for all the test runs. This laser power condition approximates synchrotron thermal heat loads for Be windows at SSRL, which sees an in situ constant heat flux due to the orbiting electrons. Coolant flow rate is measured with a stop watch and a millilitre flask.

The energy density profile of the beam is measured by covering the calorimeter aperture with a slitted mask 0.131 mm by 12.931 mm, allowing only a small fraction of the beam to pass on to the detector. Initially, the long axis of the slit is positioned on the long axis of the beam shape. Energy measurements are made for half-second illumination periods across the beam profile in the vertical direction in 0.1-mm increments. Next, the mask is turned 90°, and the measurement process is repeated in 0.5-mm increments along the horizontal axis. In either case the energy measured represents the average energy over the whole area of the slit for its relative position in the beam profile.

Figures 12A through 12F show the slit-average beam energy plotted as a function of slit position relative to the laser beam. The integrated area under the plotted curves divided by the slit width (0.131 mm) is equal to the

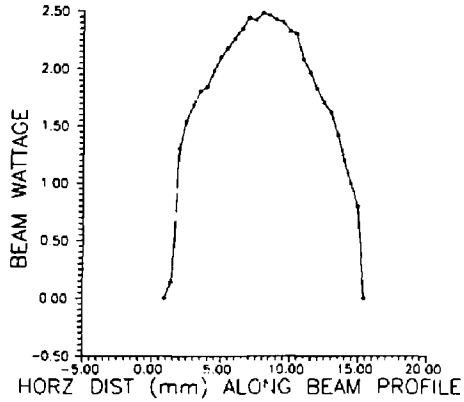

(a)

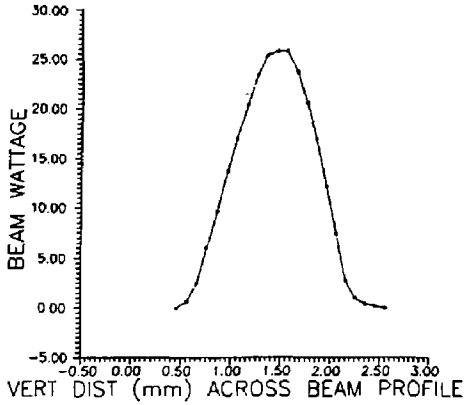

(b)

Figure 12. Plots of data for laser beam energy density profiles obtained by scanning the narrow part of a slit-mask (0.131 mm by 12.9 mm) horizontally and vertically at the focal plane of the front ideal surface of the Be window: (a) 200 W, horizontal; (b) 200 W, vertical; (c) 100 W, horizontal; (d) 100 W, vertical; (e) 87 W, horizontal; (f) 87 W, vertical.

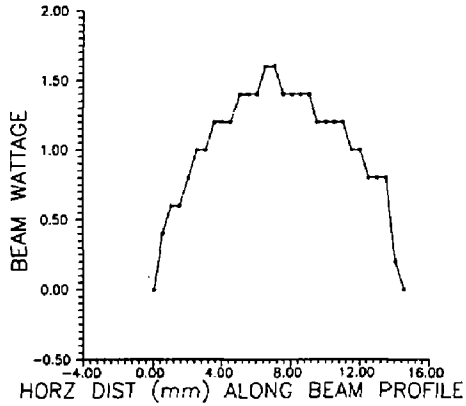

(c)

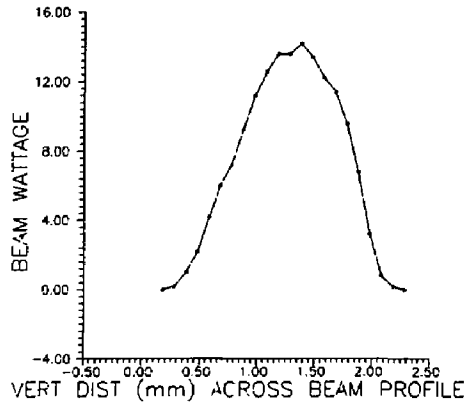

(d)

Figure 12 (Continued).

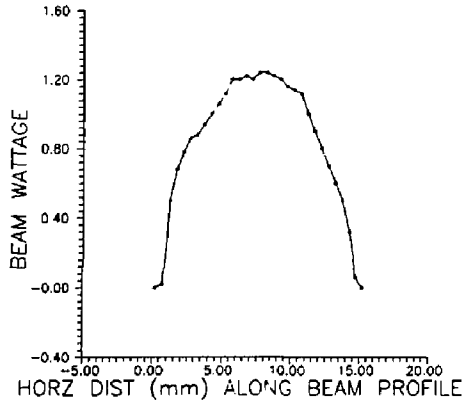

(e)

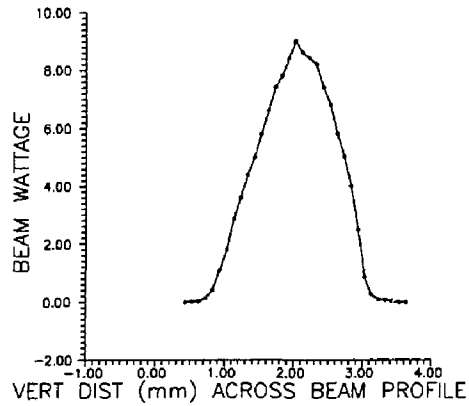

(f)

Figure 12 (Continued).

total beam energy. Similiar measured distributions, both horizontally and vertically, are seen by Be windows when subjected to synchrotron radiation thermal loads. The primary difference is that the synchrotron thermal load (i.e., with carbon filters used upstream from the Be window) is deposited almost uniformly through the thickness of the beryllium (volumetrically), whereas the laser thermally impinges the Be surface only. Without carbon filters, surface thermal loads are expected, in which case our experiment comes closer to in situ simulation. Once absorbed within the Be, most of the heat is carried away by conduction through the Be to the water-cooled copper aperture in virtually the same manner for both cases. An absorption coefficient for the Be surface at the Nd:Yag laser wavelength of 1.06 μm was not successfully measured with this experimental setup. The energy scattered within the cell could not be separated from that absorbed in the beryllium and transferred to the copper as measured by water temperature rise data coupled with the constant water flow rate.

EXPERIMENTAL PROCEDURE

Test cell preparation begins with the front and rear chambers being evacuated after flushing twice with argon. The rear chamber is then filled to 0.4 psig (15.1 psia) of helium gas. The front chamber remains evacuated at an average gage test pressure of approximately 25 millitorr argon [converted pressure of 42 millitorr for air (N_2) equivalent]. Cooling water flow rate to the test cell from the Masterflex pump is set.

To confirm the beam shape, a burn on the target block is conducted before aligning the beam onto the Be window. The data logger is set to 30-s scan intervals. The AGA Thermovision system is turned on and the camera itself is filled with liquid nitrogen along with the vacuum foreline trap.

With all preparations completed, the laser shutter is opened and the window is heated with the focused laser beam. A particular beam energy is maintained for initially a 30-min interval and repeated unless damage has been observed and additional damage is occurring slowly. If this happens, a one-hour run time interval is chosen. Visual inspection for surface damage of the Be window is made after each exposure.

OBSERVED EXPERIMENTAL RESULTS

Table 3 contains an overview of all the pertinent experimental parameters along with some calculated key parameters. Figures 13A-13E and 14A-14J are photomicrographs and scanning electron micrographs (SEM) of the associated metallographic results. Table 4 contains all the detailed data of the runs for Be windows 1, 2A, and 2B.

MECHANICAL LOADING OF THE Be WINDOWS

All three windows tested are made with 0.254-mm (10-mil) thick Be foil. Both aperture types tested had a convex side that faced the vacuum chamber; this was also the side impinged upon by the laser. This initial curvature is apparently the result of the differential contraction during the cooling portion of the vacuum brazing process of the two different materials (Be and Cu) being brazed together, plus any initial Be curvature. Beryllium window surface curvature measurements before and after laser testing revealed vertical curvature growth. Window 2B was the only one of the three windows measured before and after testing with a measured vertical curvature growth of 78%. Beryllium windows 2A and 2B had different final measured curvatures of 1.168 mm and 0.818 mm, respectively. This was evidently not a tightly controlled parameter during the fabrication process.

Surface finish before testing varied on all windows, with surface scratches apparent at all levels of magnification. These surface defects provide potential stress concentration locations for surface cracks to develop.

THERMAL DIFFERENTIAL LOADING OF THE Be WINDOWS

Large temperature gradients from the beam-impinged region on the window to the copper heat sink causes differential thermal expansion between the Be and the copper. This results in additional window distortion. For example, from the data documented in Table 3, the center thermocouple of window 2A read 381°C with 85 W impinging the Be. For the same power load the thermocouple offset 6.5 mm on the long axis registered a temperature of 173°C. The exit temperature of the cooling water was 32°C. The calculated average thermal gradient between the two thermocouples is 32°C/mm. Using the water exit temperature, a conservative estimate for the Be-copper interface is 32°C. The

Table 3. Summary of test results of the Be window thermal damage study.

Window No.	Power impinging window[a] (W)	Elapsed time at max pwr (hr)	Max temp of window center TC-5 (°C)	Max temp of window 6 mm offset TC-4 (°C)	Cooling water temp rise (°C)	Cooling water flow rate (ml/s)	Heat flux to cooling water (W)	Heat lost to the room (W)	Heat lost to the room (%)	Horiz temp grad TC-4 to TC-5 (°C/mm)	Vert temp grad TC-5 to TC-6 (°C/mm)	Vert to horiz temp grad ratio	Damage noted
1	170	0.5	352	153	18	1.57	118	52	31	31	120	3.9	Surface cracks
2A	85	3.0	381	173	14	1.20	70	15	18	31	70	2.2	Through cracks
2B	74	6.0	230	136	10	0.83	35	39[b]	53[b]	15	40	2.7	Localized surface damage

[a]The sapphire window absorbs approximately 15% of the laser power as measured by dumping a focused beam into the calorimeter with and without the sapphire window in the beam path.

[b]The insulation that was used to wrap the test cell had been removed to speed up the time to reach steady-state for each 1/2-hour run cycle for the last half of the test series on the third window.

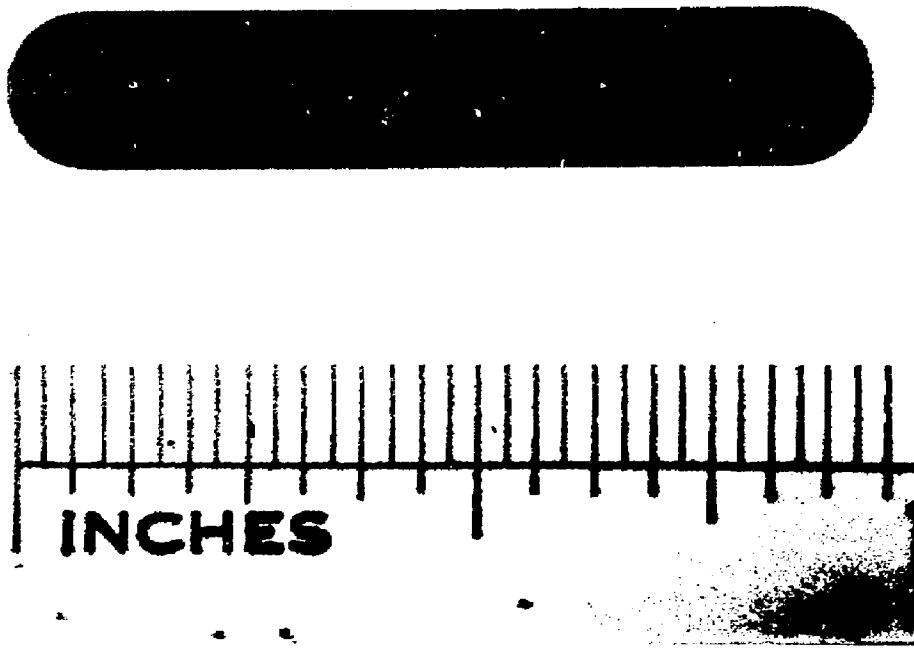

Figure 13A. Enlarged 6X macrograph of front surface of Be window 1 after 64 min of laser impingement or 384,000 pulses. The central portion shows visual signs of laser-induced surface damage. (Note: this and subsequent figures give enlargements taking 1.58X enlargement for this report into account.)

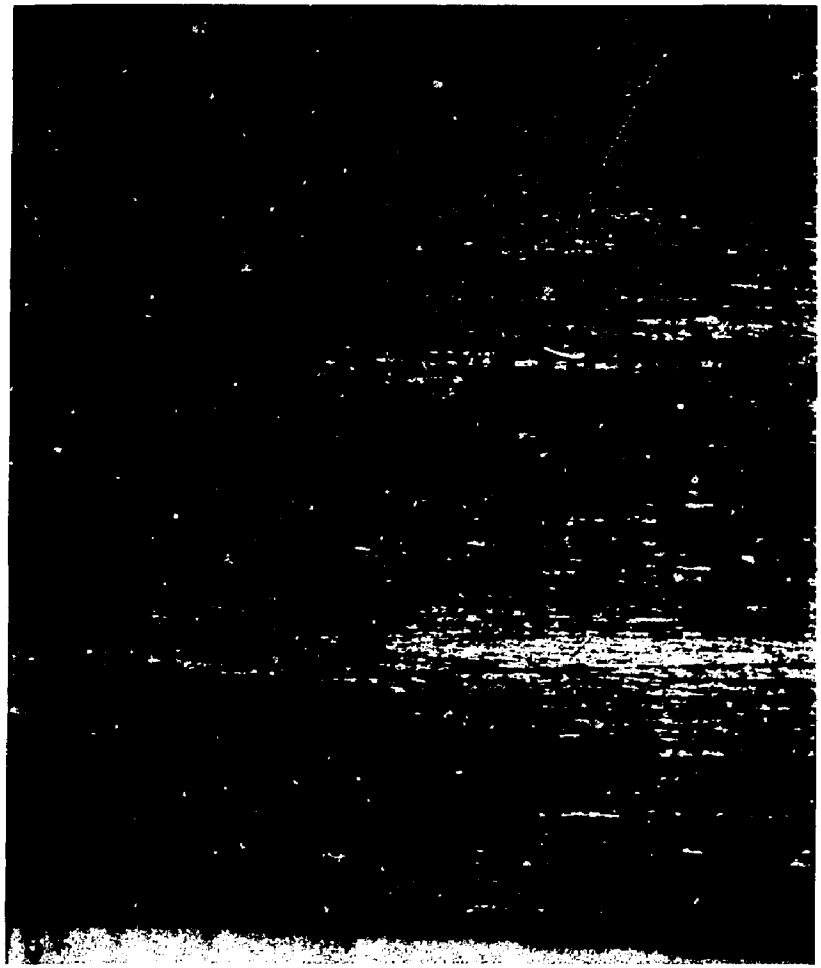

Figure 13B. Enlarged 60X photomicrograph of surface damage region of Be window 1 after 384,000 laser pulses. Surface shows signs of microcracking.

Figure 13C. Enlarged 600X SEM of surface damage region of Be window 1 after 384,000 laser pulses. At this magnification, areas of possible surface melting are visible in regions surrounding high intensities of microcracking.

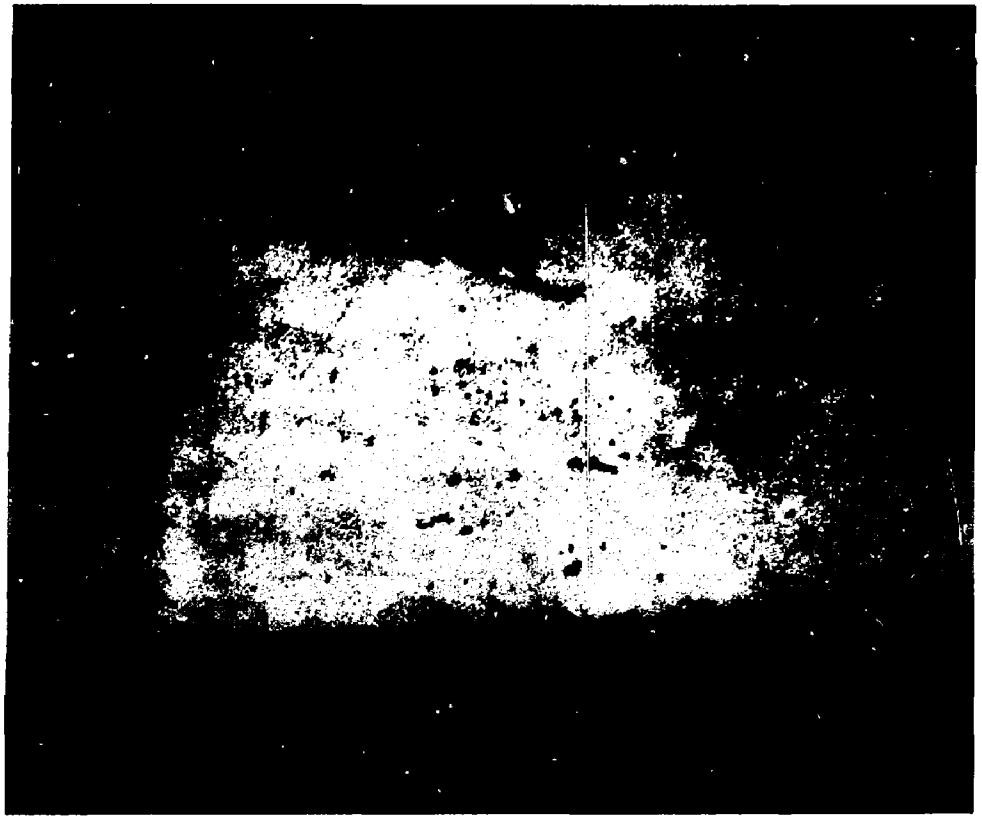

Figure 13D. Enlarged 300X photomicrograph of a transverse section showing surface damage of Be window 1 after 384,000 laser pulses. Material void imperfections associated with cracking are evident.

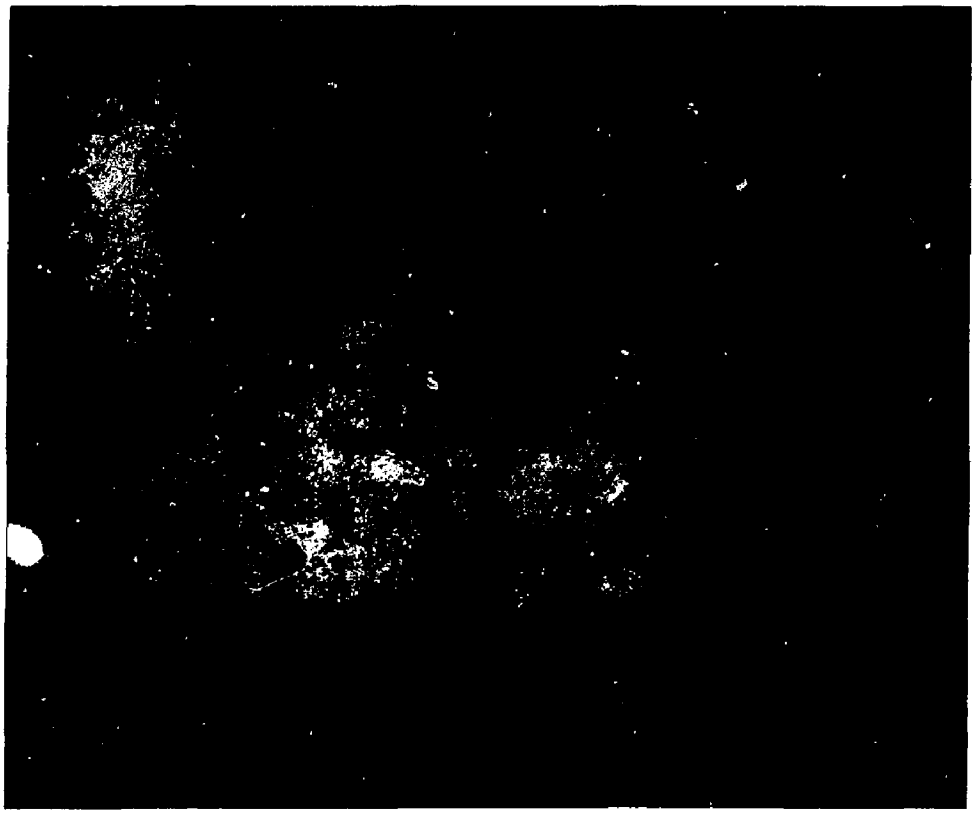

Figure 13E. Enlarged 300X photomicrograph of a transverse section showing surface damage and associated surface cracks for Be window 1 after 384,000 laser pulses.

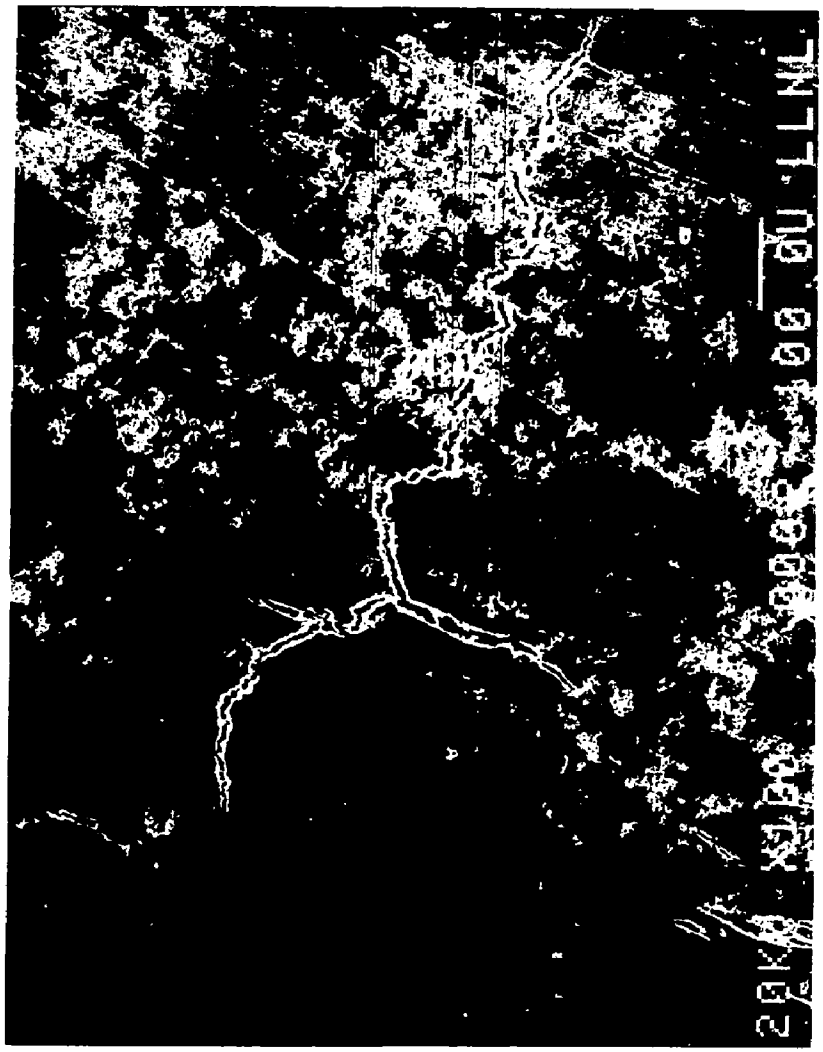

Figure 14A. Enlarged 150X SEM of front surface of Be window 2A after 181 min of laser impingement for a total of 1,086,000 pulses. Vertical crack with a smaller horizontal crack intersection shown with view rotated 30 deg. from horizontal.

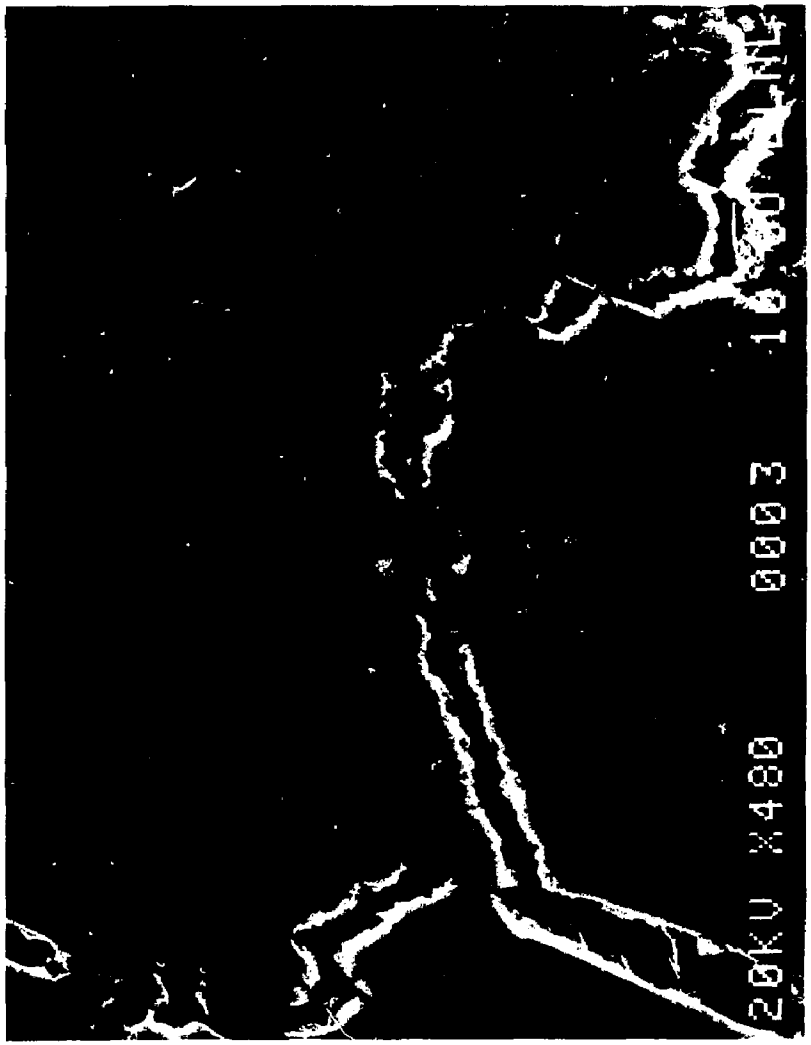

Figure 14B. Enlarged 750X SEM of front surface of Be window 2A after 181 min of laser impingement for a total of 1,086,000 pulses. Vertical crack with a smaller horizontal crack intersection shown with view rotated 30 deg from horizontal.

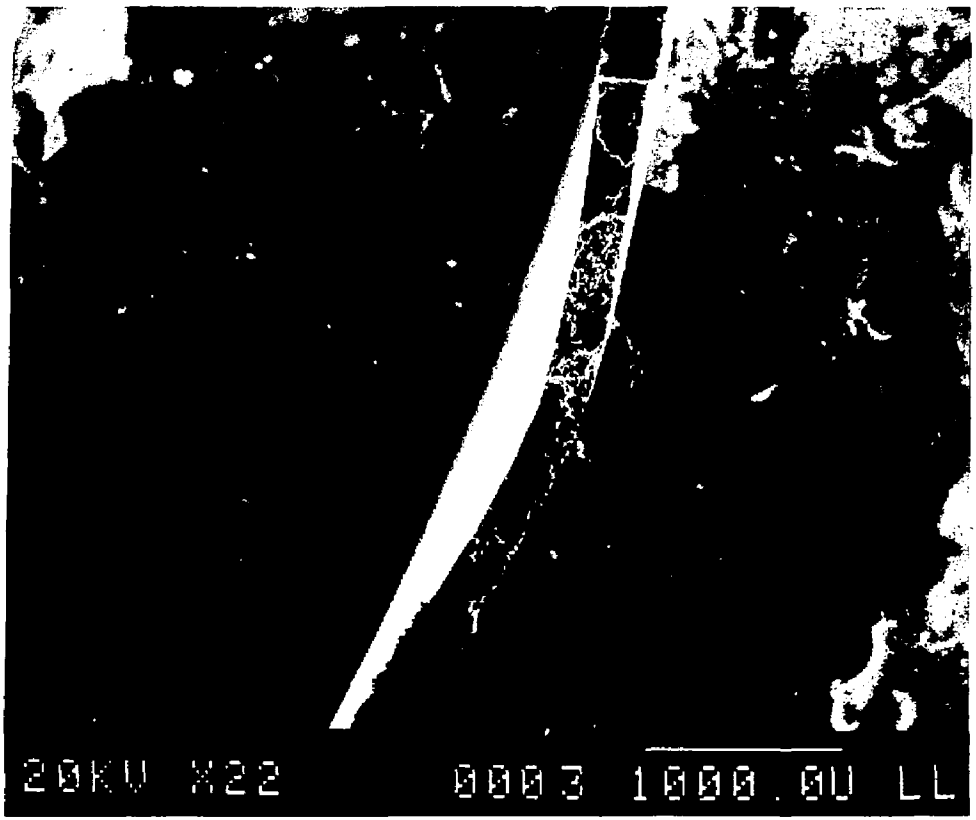

Figure 14C. Enlarged 35X SEM of vertical crack surface of Be window 2A after 1,086,000 laser pulses. Crack is split open exposing the vertical crack surface shown with very different surface texture within (lower) and outside (upper) the area impinged by the laser beam. The crack surface within the focused laser beam shows signs of surface melting.

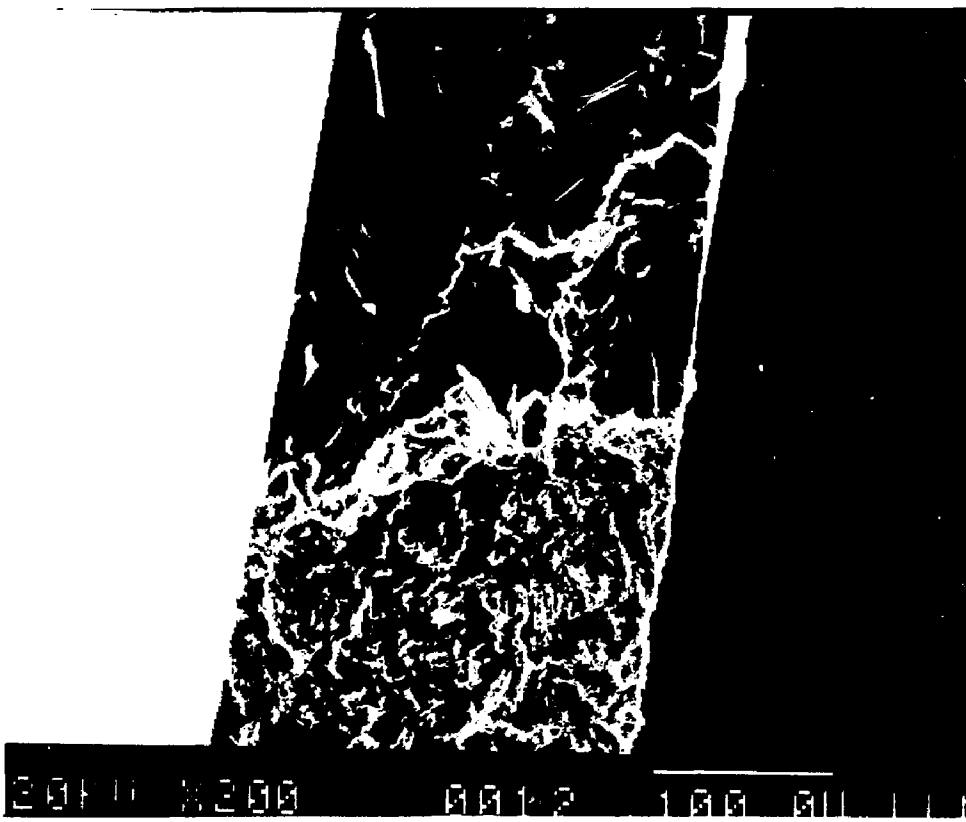

Figure 14D. Enlarged 300X SEM of vertical crack surface of Be window 2A after 1,086,000 laser pulses. Crack is split open exposing the vertical crack surface shown with very different surface texture within (lower) and outside (upper) the area impinged by the laser beam. The crack surface within the focused laser beam shows signs of surface melting.

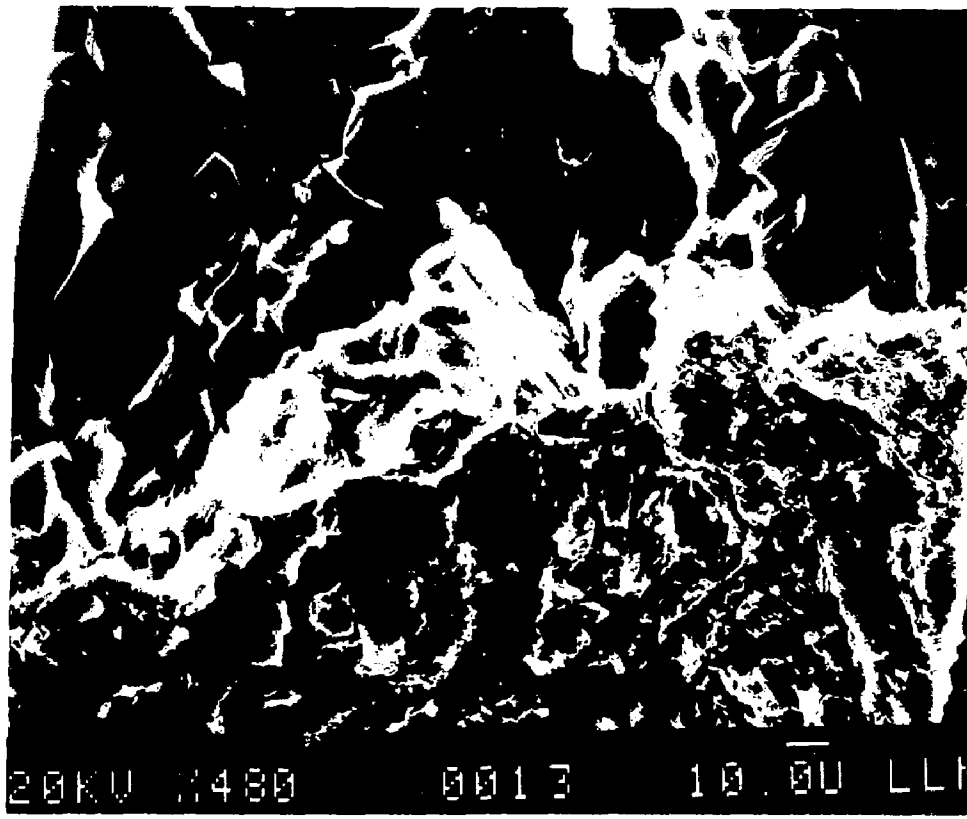

Figure 14E. Enlarged 750X SEM of vertical crack surface of Be window 2A after 1,086,000 laser pulses. Crack is split open exposing the vertical crack surface shown with very different surface texture within (lower) and outside (upper) the area impinged by the laser beam. The crack surface within the focused laser beam shows signs of surface melting. In the upper area, careful observation shows crack surface microcracking.

Figure 14F. Enlarged 1570X SEM of vertical crack surface of Be windown 2A after 1,086,000 laser pulses. Crack is split open exposing the vertical crack surface shown with crack surface microcracking easily observed outside the focused laser beam.

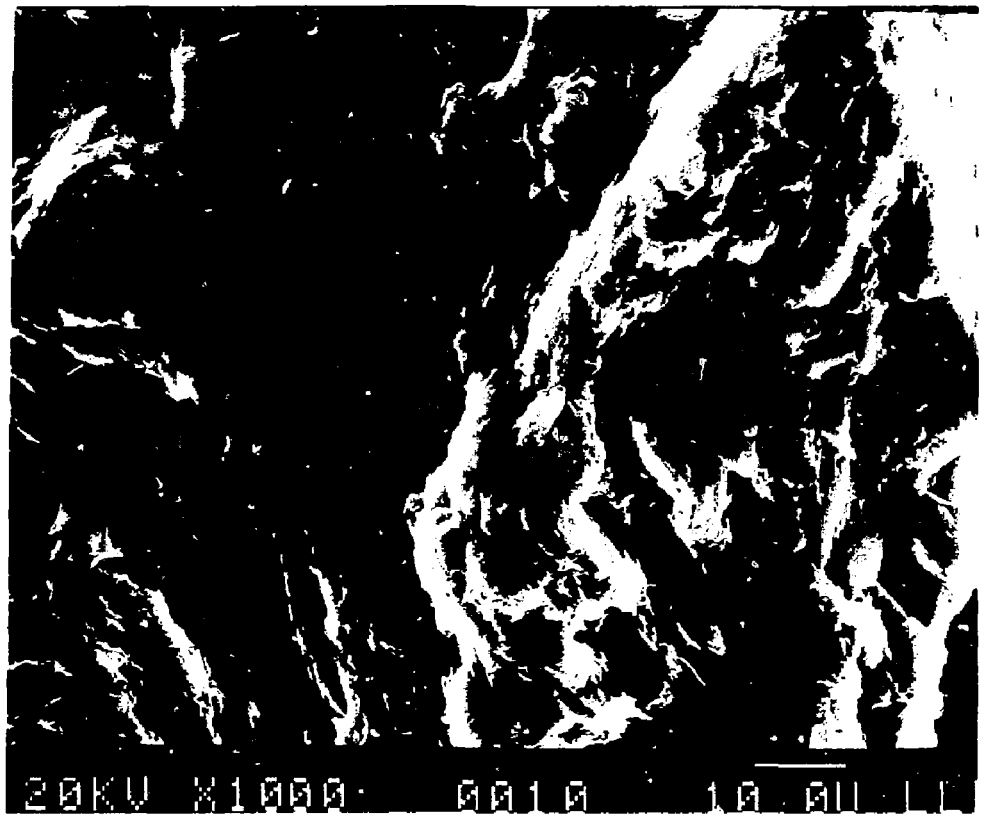

Figure 14C. Enlarged 1570X SEM of vertical crack surface of Be window 2A after 1,086,000 laser pulses. Crack is split open exposing the vertical crack surface shown under the area impinged by the laser beam. The crack surface shows signs of surface melting.

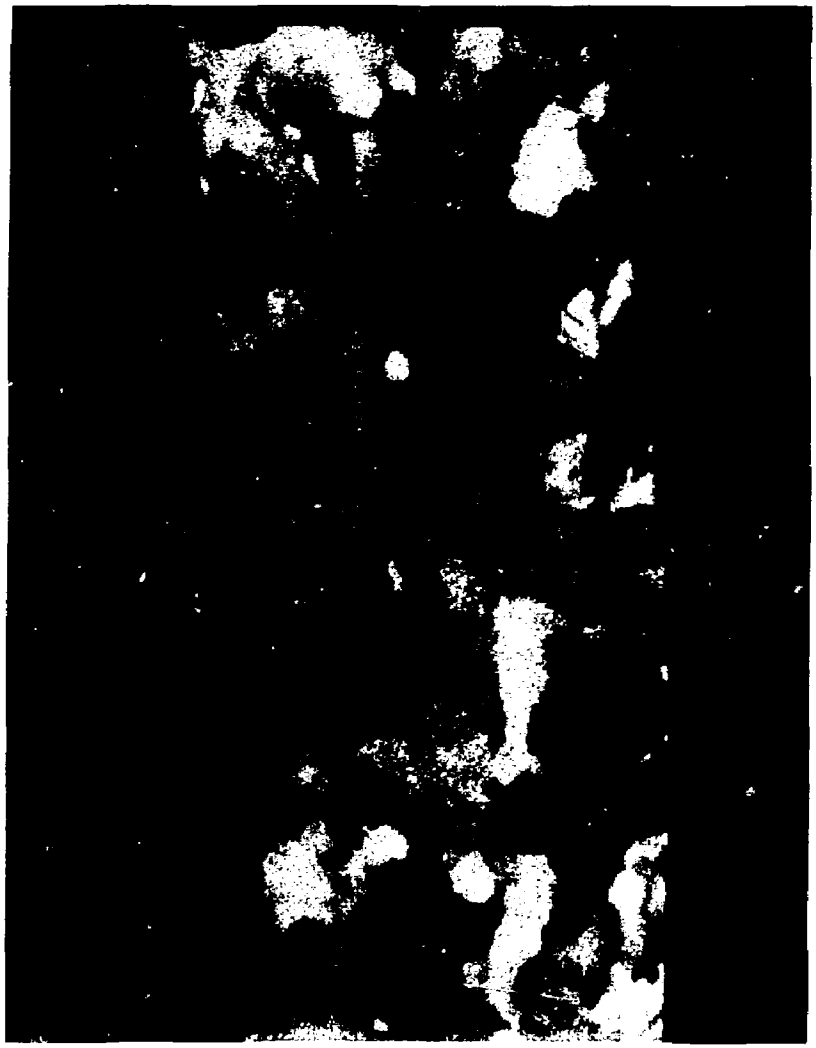

Figure 14H. Enlarged 300X transverse polished photomicrograph section of Be window 2A after 1,086,000 laser pulses showing horizontal crack at the apex.

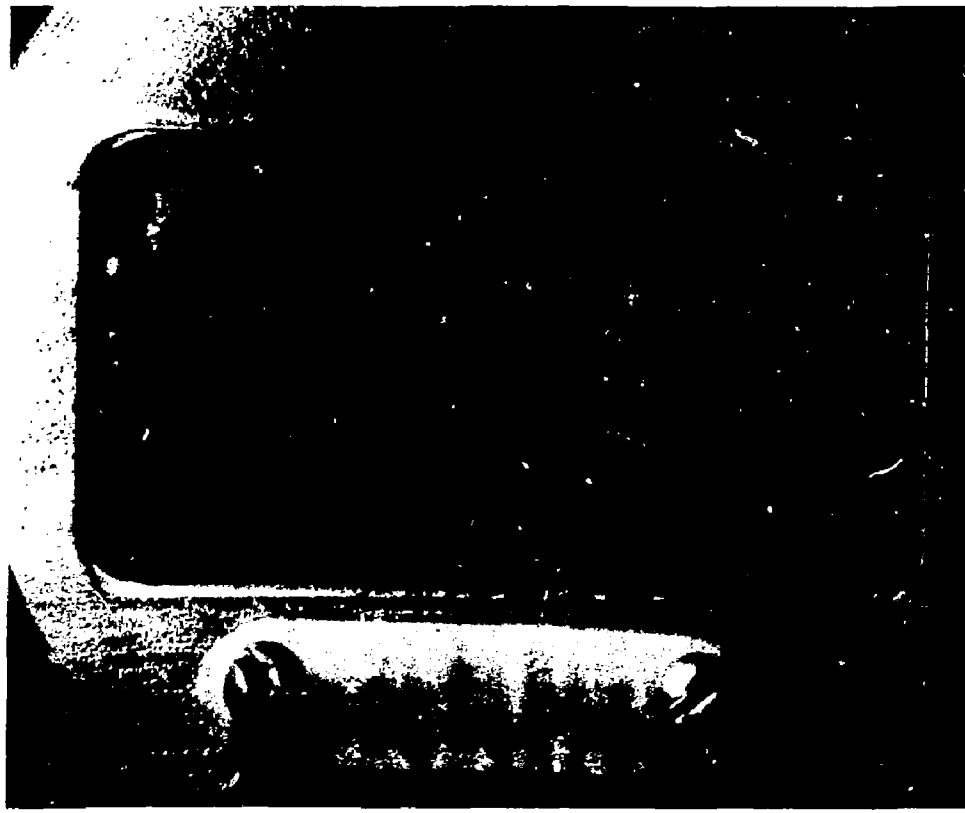

Figure 14I. Beryllium window enlarged 6X showing 0.001-in. thermocouple wires laser welded to the back surface of Be foil. Thermocouple TC-4 is mounted 6.5 mm from center and thermocouple TC-5 is mounted directly in the center that corresponds to the peak laser-impinged flux on the front surface.

Figure 14J. Beryllium window 2A showing 300X polished photomicrograph section of the thermocouple spot welded to the back Be surface. A good joint was obtained giving confidence to the measured thermocouple temperature readings.

Table 4. Detailed beryllium test data for windows 1, 2A, and 2B.

	Window 1		Window 2A				Window 2B				
Thickness (mm)	0.254		0.269				0.257				
Curvature - measured from true flat (mm)	Unknown		Note: Measured after testing 1.168				Measured: Before Test: 0.457 After Test: 0.818				
Aperture (mm)	5 wide x 25 long		10 wide x 25 long				10 wide x 25 long				
Grain direction	Along length of window (horiz.)		Along length of window (horiz.)				Approx. 15° off length of window (horiz.)				
Forward chamber vacuum (mT-Argon)	122	65	64	30	27	37	9	9	9	6	6
Rear chamber pressure (atm-Helium)	1.03	1.03	1.03	1.03	1.03	1.03	1.03	1.03	1.03	1.03	1.03
Date	3/26	3/27	4/8	4/9	4/9	4/9	4/16	4/17	4/17	4/17	4/20
Laser power (W)	100	200	100	100	100	100	100	50	50	50	75
Time (hr : min)	15:28 16:03	9:40 10:09	13:23 13:52	9:53 10:23	12:29 13:28	13:55 14:58	12:43 12:50	9:13 9:42	10:06 10:39	11:52 12:53	10:54 11:24
Peak T. C. centerline Temperature °F	294	666 653	586	651	712	718	415	276	268	262	390
H_2O flow (ml/min)	47	47 94	50	72	72	72	44	44	44	44	44
Mode of failure	N.A.	N.A.	N.A.	N.A.	N.A.	Leak[a]	N.A.	N.A.	N.A.	N.A.	N.A.
Visual inspection	None	Surface damage. Photo macro-graphs taken & window sectioned	Small horiz. Edges look like delamin-ating orange peel	Cracks more pro-nounced. Grain in beam profile washing out	Surface pitting. Dull vs shiny areas around crack lengths	Photo macro-graphs taken & window sectioned	None	None	None	None	Small dark trangular spot appeared with lines eminating from it

[a]Upon cooldown leak developed almost immediately after laser shut-off (20 μm leak).

57

ndow

6	6	6	6	6	6	6	4	4	7	4	5	4 to 7	4 to 7	4 to 7
1.03	1.03	1.03	1.03	1.03	1.03	1.03	1.03	1.03	1.03	1.03	1.03	1.03	1.03	1.03
4/17 50	4/20 75	4/20 75	4/21 75	4/21 75	4/21 87.5	4/21 87.5	4/21 87.5	4/21 87.5	4/21 87.5	4/21 87.5	4/22 87.5	4/22 87.5	4/22 87.5	4/22 87.5
11:52 12:53	10:54 11:24	14:20 14:50	8:58 9:16	9:27 10:00	10:15 10:45	10:55 11:25	11:35 12:05	1:36 2:08	13:20 13:50	14:07 14:37	8:16 8:46	8:55 9:55	10:01 10:31	13:20 14:20
262	390	490 393	363	378	437	432	431	430	425	435	438	442	439	446
44	44	44 96	96	50	50	50	50	50	50	50	50	50	50	50
N.A.	N.A.	N.A.	N.A.	N.A.	N.A.	N.A.	N.A	N.A.	N.A.	N.A.	N.A.	N.A.	N.A.	N.A.
None	Small dark trangular spot appeared with lines eminating from it	Nothing more	Same	No change	Maybe more grain distinc-tion.	Rolling grain in laser beam foot print 40-50% visible	Micro cracking 2X & 3X	Cracks are darker	No change	Cracks are getting more defin-tion and clarity	Cracks are extend-ing left and right of beam center line	No change	No change	Photo macro-graphs taken & window sectioned.

average thermal gradient from the offset thermocouple to the Be-copper interface 6 mm horizontally on the long window axis is calculated at 23.5°C/mm for window 2A. Thermal gradient along the short axis from center thermocouple to Be/copper interface is 70°C/mm. The corresponding laser beam power gradients derived from the maximum slopes of the measured power distributions in Figs. 12C and 12D are 135 W/mm vertically and 2.3 W/mm horizontally.

The Be window accommodates the large thermal/mechanical stresses by growing/stretching. Pretest/posttest measurements show approximately 78% vertical curvature growth of window 2B at its center. A crack along the long axis of window 2A was first observed after the first 30-min run just below the beam illumination profile where the thermal gradient was the greatest. Window failure happened immediately after beam shutdown after three hours of running or approximately 1,000,000 pulses (two runs at 30 min and two runs at 60 min) and subsequent cooling. Failure was noted by the rise in pressure on the vacuum side of the window. Although horizontal cracks were observed before failure, inspection after failure revealed a small vertical crack on the front and rear surface of the window. None of the horizontal cracks appeared on the rear of the window.

Scanning electron microscope (SEM) photographs and micrographs (figure series 13A-E and 14A-J) show cross sections of the crack topography. The Be beneath the beam pattern shows an elevated temperature quasi-cleavage failure, while just outside the material failed by intergranular cleavage.

RELATING LASER HEATING TO SYNCHROTRON RADIATION HEATING OF THE BERYLLIUM WINDOWS

In actual operating conditions the Be windows are exposed to synchrotron radiation that heats the window volumetrically. Laser irradiation heats only the surface. However, we can relate our results to actual operating conditions by analyzing how the heat flows from the beryllium to the copper heat sink. The material property of the beryllium that relates how transient heat is conducted from either heated area to the sink is called the thermal diffusivity. Thermal diffusivity is equal to the material's thermal conductivity divided by the product of its density and specific heat. For the laser-heated beryllium window, the time required for the unilluminated back surface to reach half of the maximum temperature rise was calculated to be approximately 2 to 4 ms as compared with the average laser pulse width of

1.2 ms. From the characteristic thermal response times involved, the window experienced close to steady-state thermal input conditions, as it does in the synchrotron line.

The maximum temperature recorded on the back side was 381°C. Front surface temperatures can only be 10 to 20 degrees higher because of the high thermal conductivity of the beryllium and the short heat transfer distance. However, some of the surface grains on the front surface of the Be foil reached higher temperatures, even approaching the melting point as they were separated from the parent material by microcracking. Examples are evident in the SEMs and photomicrographs.

Window 2A's stress cracking was first observed to occur after the first half hour exposure (with 85 W impinging it) at approximately 180,000 pulses. Failure occurred 2-1/2 hours (approximately one million laser pulses) later at the same beam settings. Average beam density was 3 W/mm^2 with a peak center density of 5 W/mm^2. SEM photographs indicate subgranular melting, but metallography macrographs do not reveal any change in grain size, although the heat-affected zone of the second window shows a finer surface structure on the crack surface.

CONCLUSIONS

An experimental study to investigate thermal-induced damage to SSRL-designed beryllium foil windows was performed at LLNL's Laser Welding Research Facility. The primary goal of this study was to determine the threshold at which thermal-stress-induced damage occurs in these commonly used vacuum barriers. An Nd:Yag pulsed laser with cylindrical optics and a carefully designed test cell provided a test environment that closely resembles the actual beamline conditions at SSRL. Tests performed on two beryllium window geometries, with different vertical aperture dimensions but equal foil thicknesses of 0.254 mm, resulted in two focused total-power thresholds at which incipient damage was determined. For a beam spot size similar to that of the Beamline-X Wiggler Line, onset of surface damage for a 5-mm by 25-mm aperture window was observed at 170 W after 174,000 laser pulses (1.2-ms pulse at 100 pps).

A second window with double the vertical aperture dimension (10 mm by 25 mm) was observed to have surface cracking after 180,000 laser pulses with 85 W impinging its front surface. Failure occurred 2-1/2 hours (approximately one

million laser pulses) later at the same 85 W setting. Another window of the same type (10 mm by 25 mm) received 2,160,000 laser pulses at 74.4 W with subsequent metallographic sectioning revealing no signs of through-thickness damage. Comparison of windows with equal foil thicknesses and aperture dimensions has effectively identified the peak heat flux limit, 3 to 5 W/mm^2, for incipient failure. The existing SSRL thermal flux operational limit for all Be windows is 3.75 W/mm. We observed damage at 3.6 W/mm (5 W/mm peak averaged over a 14-mm beam length) for a 10-mm by 25-mm aperture. Therefore the existing limit should not be exceeded until an exact understanding of the wiggler beamline in situ window temperatures are measured under actual operating conditions.

The data show that halving the aperture's vertical dimension allows doubling the total incident power for equivalent onsets of thermal-induced damage. Future window designs should decrease the vertical aperture dimension as much as possible.

FUTURE STUDIES

To increase the quantitative understanding of window failure, future work will include in-situ temperature measurement under actual beam operating conditions.

Future studies should include 2-D and 3-D thermal stress analysis of the above results combined with other possible window geometries and loadings. These studies should include the nonisotropic material properties of the Be foil material.

Also, a study should be directed at predicting the fatigue life of these windows, since they experience daily temperature cycles. Surface cracks both from manufacturing and thermally induced will play a key role in the failure of these windows.

ACKNOWLEDGMENTS

We wish to thank several members of the LLNL Mechanical Engineering Department staff for their valuable assistance in the Be Window Damage Study. They include MFED's Laser Welding Facility operators: Calvin Anglin, Mark Gauthier, James Murchie, and Carl Westrich, all of whom made significant contributions in assembly, implementation, calibration, and operation, along

with many very useful suggestions for improving the experiment. James Ferreira provided metallurgical support during experimental runs. Allen Lingenfelter provided the manpower and facility to perform the experimental part of this study. William Goodman provided the original design concept for the test cell, which was skillfully fabricated and assembled by Albert Knabe. John Lietzke and Gregory Bianchini provided ancillary equipment. We also wish to thank members of the LLNL Chemistry and Materials Science Department for their assistance. Sam Digiallonardo and Robert Meisenheimer generated metallurgical data. Interpretation was provided by Fred Fulton and James Hanafee.

Glenn Tirsell provided interpretations of expected beam thermal profiles for Beamline-X as well as guidance on physics objectives. Satish Kulkarni gave all of us essential guidance and direction to achieve success in this study. We wish to thank Carl Poppe for his support. We also appreciate the encouragement of A. Bienenstock and H. Winnick of SSRL.